Material properties and empirical rate equations for hydrogen sorption reactions in 2 LiNH2–1.1 MgH2–0.1 LiBH4–3 wt.% ZrCoH3

Material properties and empirical rate equations for hydrogen sorption reactions in 2 $LiNH_2$ – 1.1 MgH_2 - 0.1 $LiBH_4$ - 3 wt.% $ZrCoH_3$

I. Bürger[1], J.J. Hu[2], J. G.Vitillo[3],G.N.Kalantzopoulos[4], S. Deledda[4], M. Fichtner[2], M. Baricco[3], M. Linder[1]

[1] Institute of Technical Thermodynamics, German Aerospace Center (DLR), D-70569 Stuttgart, Germany, email: inga.buerger@dlr.de

[2] Institute of Nanotechnology, Karlsruhe Institute of Technology (KIT), D-76021 Karlsruhe, Germany

[3] Dipartimento di Chimica and NIS, Università di Torino, Via P.Giuria 7-9, I-10125 Torino, Italy

[4] Institute for Energy Technology, Physics Department, P.O. Box 40, NO-2027, Kjeller, Norway.

Abstract

2 $LiNH_2$ –1.1 MgH_2 - 0.1 $LiBH_4$ - 3 wt.% $ZrCoH_3$ is a promising solid state hydrogen storage material with a hydrogen storage capacity of up to 5.3 wt.%. As the material shows sufficiently fast desorption rates at temperatures below 200 °C, it is used for a prototype solid state hydrogen storage tank that is coupled to a HT-PEM fuel cell. In order to perform design simulations for this prototype reactor with a hydrogen capacity of 2 kWh_{el}, model equations for the rate of hydrogen sorption reactions are required. Therefore, several material properties, like bulk density and thermodynamic data, have been measured. Furthermore, isothermal absorption and desorption experiments are performed in a temperature and pressure range that is in the focus of the coupling system. Using experimental data, two-step model equations have been fitted for the hydrogen absorption and desorption reactions. These empirical model equations are able to capture the experimentally measured reaction rates and can be used for model validation of the design simulations.

Keywords

Li-Mg-N-H hydride; reaction rate; model equations; hydrogen storage

1 Introduction

Due to high theoretical storage densities, complex hydrides show the potential to improve the present state of the art of hydrogen storage for automotive applications [1]. As the hydrogen is strongly bonded to the powdered material, the amount of free gaseous hydrogen in equilibrium at room temperature and pressure is small. Therefore, hydrogen is just released when external heat is provided for the endothermal desorption reactions. In case the storage reactor is coupled to a fuel cell (FC), the required amount of hydrogen can be released by transfer of the waste heat from the FC. This kind of coupled system has already been studied by several simulations and experiments for conventional metal hydrides, as well as for $NaAlH_4$ [2–4].

The present work has been developed within a framework of activities aiming to realize a hydrogen storage tank that is studied in technically relevant scale, i.e. allowing for 2 h coupled operation with a 1 kW_{el} high temperature proton-exchange membrane (HT-PEM) fuel cell. As for an appropriate tank design modelling simulation tools are used, reliable information on the properties of the selected storage material are required, e.g., bulk density, storage capacity, thermodynamic properties and

reaction rate equations. In the present paper, these values are summarized for the selected material. Studies on the absorption and desorption performance of lab-scale reactors using this material can be found in [5,6]. The material that has been chosen for the prototype system is based on the Li-Mg-N-H system, as these materials release significant amounts of H_2 at temperatures below the HT-PEM fuel cell operating temperature, i.e. max. 200 °C [7]. Thus, it is possible to maintain the tank at a temperature sufficiently high for good hydrogen delivering rates by simply using waste heat of the fuel cell. Although the Li-Mg-N-H system has been suggested for hydrogen storage in automotive applications previously [8], to our knowledge, applications have not been reported yet.

While pure Li-N-H stores theoretically 11.5 wt.% [9], the partial substitution of LiH with MgH_2 reduces the amount of H_2 to 5.4 wt.% [10]. However, this substitution significantly reduces the thermodynamic barriers [11,12], and an experimental gravimetric density of 4.6 wt.% below 200 °C can be reached [10]. In the basic system for this study, the ratio of Lithium Amide to Magnesium Hydride is 2:1.1, and the reaction of this system is reported as [10,13]

$$2\mathrm{LiNH_2}+\mathrm{MgH_2} \underbrace{\rightarrow}_{1} \mathrm{Mg(NH_2)_2}+2\mathrm{LiH} \underbrace{\rightleftharpoons}_{2} \mathrm{Li_2Mg(NH)_2}+2\mathrm{H_2}. \qquad (1)$$

The first step (1) is an irreversible exothermic metathesis reaction that just takes place during the first “activation“ procedure. The corresponding reaction enthalpy has been estimated by Araújo et al. as 68.8 $kJmol^{-1}$ [14] and experimentally verified by Luo [15]. The storing processes corresponds to the second reaction (2), that reversibly absorbs/desorbs hydrogen in two steps (2a and 2b). These steps have been verified by in-situ neutron diffraction [16] and can be written as

$$2\mathrm{Li_2Mg(NH)_2}+4\mathrm{H_2} \underbrace{\rightarrow}_{2a} \mathrm{LiH}+\mathrm{LiNH_2}+\mathrm{Li_2Mg_2(NH)_3} \underbrace{\rightarrow}_{2b} 4\mathrm{LiH}+2\mathrm{Mg(NH_2)_2}. \qquad (2)$$

The first step (2a) appears in PCI curves as a sloping region, while the second step (2b) corresponds to a plateau [10].

In order to improve this basic system, different additives have been investigated in the literature. $LiBH_4$ seemed to improve reaction rates and thermodynamics, when added in small ratios [17,18]. In 2010, Zhang et al. presented a system with 2-1.1-0.1 $LiNH_2$-MgH_2-$LiBH_4$ and 3 wt.% $ZrCoH_3$, showing a theoretical hydrogen capacity of 5.6 wt.% and experimentally observed capacities of 5.3 and 3.75 wt.% for absorption and desorption, respectively [19]. Ulmer et al. studied the same system resulting in capacities of 3.5 to 4.2 wt.% [20]. According to Hu et al. [21], the effects of the two additives in this basic system are different. While the addition of $LiBH_4$ facilitates the metathesis reaction for the first cycle and furthermore generally enhances kinetics via the formation of a liquid intermediate phase, $ZrCoH_3$ leads to powder pulverizing effects. For the development of the prototype reactor, this material has been chosen due to the acceptable storage capacity and sufficient reaction rates below 200 °C. In the following, this material will be abbreviated as Li-Mg-N-H.

So far, in literature there do not exist model equations describing the reaction rates of this material for absorption and desorption, but rather qualitative comparative studies on the reaction rates using different dopants [17,21,22]. Thus, in the present paper, the focus is on the determination of simple but satisfying mathematical equations describing the reaction rate of the absorption and desorption process of the material in the desired pressure and temperature range. Furthermore, thermodynamic data, as well as bulk density, will be determined.

2 Experimental

2.1 Material preparation

$LiNH_2$ (95%, Sigma-Aldrich), MgH_2 and $LiBH_4$ (95%, Alfa Aesar) were purchased, stored in the glove box and used as received without pretreatment. $ZrCoH_3$ was prepared from ZrCo ingot (SAES Getters S.p.A., Italy) by exposing to 1 MPa H_2 at ambient temperature and milled before use.
The starting chemicals with a composition of $2LiNH_2$-$1.1MgH_2$-$0.1LiBH_4$-3 wt.% $ZrCoH_3$ were loaded into a 500 ml milling vial made of stainless steel and sealed inside the glovebox. Ball milling was conducted on a Retsch PM-400 planetary ball mill that can accommodate 4 milling vials in one run. Each vial contained 103 g of material, so that in total 412 g material was prepared in a single batch. The milling was operated at 250 rpm in a reverse mode at the interval of 10 min / 1 min for 100 h with a ball-to-powder ratio of 5.

2.2 Activation procedure

After synthesis, the material is still present in the basic form as Lithium Amide and Magnesium Hydride with only a small fraction reacted to $Li_2Mg(NH)_2$. Therefore, before the material is studied for hydrogen sorption, the powder needs to be transformed by an exothermic *metathesis reaction* (see Equation 1) that causes a visible change in material colour from dark black to light grey.
For small amounts of material this is usually done by applying a slow heating ramp (2-5 $Kmin^{-1}$) or just by cycling the powder in an isothermal measurement setup. However, for larger amounts (2 g or even kg scale for the final prototype), it is not possible to keep the reaction bed at isothermal conditions. In contrast, the reaction of the material is accelerating due to the heat evolution of this metathesis reaction. Therefore, the activation of the material needs to be performed very carefully for larger volumes of materials and heat removal needs to be addressed by ,e.g. heating up the material in isothermal steps of several hours for every 10 K.

2.3 Density

As He pycnometry is a suitable method to obtain the density of powder samples at room temperature [23], this method has been applied to the selected Li-Mg-N-H material. The He pycnometry measurements have been performed in a home-made, well-calibrated Sieverts apparatus. Expansions of He (purity 6.0) from a reservoir volume to the sample holder took place five times, and the maximum pressure was kept under 4 bar to minimize the effect of the gas compressibility.

2.4 PCI measurements

Hydrogen sorption experiments were performed in the 0–100 bar pressure range using a volumetric instrument (PCI instrument by Advanced Materials Corporation, Pittsburgh PA). Ultra-pure 6.0 grade H_2 was used and the powders (about 500 mg) were transferred under nitrogen atmosphere in the measurement cell. For PCI measurements (performed at 170, 180 and 200°C), the sample was previously activated by three cycles of absorption (100 bar)/desorption (vacuum) at 150°C. For each PCI run, new sample material has been used.

2.5 Testing setup for measurement of reation rates

For the measurements of the reaction rates, a reactor has been designed for approx. 2 g of material. The main requirement for this reactor has been to guarantee isothermal and isobaric reaction conditions over the powder bed. Thus, any heat or mass transport limitations that could affect the measured reaction rate have been avoided. This has been realized by the following three points [24]:

- The contact surface with the surrounding stainless steel has been designed to be as large as possible to enhance heat removal and avoid hot spots inside the powder bed.
- The stainless steel mass of the reactor is big enough to limit the temperature increase to a maximum of ΔT = 2 K inside the stainless steel material, while taking up the total heat of reaction of the powder.
- The amount of material inserted into the reactor has to be adapted to absorb 0.1 g H_2, leading to a sufficient measurement accuracy for evaluation of conversion.

As shown in Figure 1, the final geometry of the reactor is a spindle with a gap of 0.5 mm. The reactor can then be filled by screwing the spindle into the powder material. In order to control the temperature, one thermocouple is integrated into the reactor and placed close to the powder.

For the hydrogen sorption experiments, this reactor has been integrated into the setup shown in Figure 1. The general principle of this setup is a volumetric measurement based on the measured pressure difference in a known reference volume before and after the experiment (Sieverts type) [25]. Before the experiment starts, in the known Sieverts volume (V_s + V_{abs} + V_{des}) a certain pressure (PS4) is applied. Furthermore, the temperature in the reactor is controlled by a thermostatic bath at the defined set temperature. Then, for absorption the manual valve HV-3 is closed in order to maintain the set pressure in the small volume V_{abs}. After opening the pneumatic valve PV-2, the gas is flowing into the reactor (V_R) and the absorption reaction is initiated: On one side of the differential pressure sensor (in V_s+V_{des} +V_R), the pressure decreases until the reaction is complete, due to the void volume of the reactor and due to the absorption reaction inside of the reactor. While on the other side of the sensor in V_{abs} the pressure is constant. Hence, the pressure difference between these two volumes can be measured and it corresponds to the absorbed mass of hydrogen. This pressure difference reached maximum values of 2 bar in the present experiments, while the pressure variation between two experiments was 15 bar for absorption and 3 bar for desorption. Thus, the present experiments can be considered reasonably isobaric. In case of desorption, the same procedure is inversed: HV-2 is closed and the pressure is increasing in V_S + V_{abs}.

3 Results and Discussion

In the following, the results of the important properties of the Li-Mg-N-H material for reactor design simulations are presented and summarized.

3.1 Bulk properties

The material density is a very important property in order to estimate the volume the material occupies in the reactor and thus an important input parameter for the reactor design simulations. Using the setup described in Section 2, the density of the as-milled sample has been determined to be $1.00 \cdot 10^3$ kgm^{-3} The sample was afterwards heated up to 500 °C at 2 °C/min and was kept isothermally

for 8 h under dynamic vacuum. Then, it was let to cool down to room temperature where pycnometry measurements took place. Its density in the desobed state was $0.79 \cdot 10^3$ kgm^{-3}. These values are in accordance with literature values of $0.54 \cdot 10^3$ kgm^{-3} for the bulk density, when an open porosity of 50 to 60% is assumed [26].

3.2 Thermodynamic properties

As during lab-scale experiments high equilibrium temperatures (220-250 °C) have been reached at pressures of 70 or 85 bar, experimental PCI measurements as well as results from experimental lab-scale reactor have been used for the determination of the thermodynamic parameters. From the corresponding van't Hoff plot, the enthalpies ($\Delta_R H$) of the sorption reactions are $\Delta_R H_{abs}$ = -38 kJ·mol$^{-1}_{H2}$ and $\Delta_R H_{des}$ = 45 kJ·mol$^{-1}_{H2}$, and the entropies ($\Delta_R S$) of the reactions are $\Delta_R S_{abs}$ = -111 J·mol$^{-1}_{H2}$·K^{-1} and $\Delta_R S_{des}$ = 124 J·mol$^{-1}_{H2}$·K^{-1} for absorption and desorption, respectively. These values are in good agreement with those reported in ref. [27].

3.3 Reaction rates

In order to simulate basic absorption or desorption scenarios in a reactor, the reaction rate of the material is necessary. Therefore, empirical equations for the absorption and desorption of the present Li-Mg-N-H material have been developed and the according results are summarized in this section.
The procedure that is used for the fitting of all rate equations is based on the assumption that the effective reaction rate can be described by the following equation

$$\frac{\partial x}{\partial t} = -\underbrace{A \cdot \exp\left(-\frac{E_a}{\mathfrak{R}T}\right) \cdot f(P)}_{k} \cdot f(x), \tag{3}$$

where x is the transformed fraction, t is the time and P is the gas pressure. The first factor on the right hand side refers to the Arrhenius equation describing the *temperature dependency* of the reaction rate, where A is the pre-exponential factor, E_a is the effective activation energy and $\mathfrak{R}$ is the gas constant. The second factor represents the *thermodynamic information* by a dependency of the rate on the distance to the equilibrium pressure. For this factor, two basic mechanisms which are common for metal hydrides according to [28,29] or [30,31]

$$f(P) = \left(\frac{P - P_{\mathrm{eq}}}{P_{\mathrm{eq}}}\right), \text{ or} \qquad f(P) = \ln\left(\frac{P}{P_{\mathrm{eq}}}\right), \tag{4}$$

have been used, where P_{eq} is the equilibrium hydrogen pressure. As indicated in Equation 3, the product of the Arrhenius and the pressure factor is also referred to as rate coefficient k.
The last factor on the right hand side of Equation 3 is a function representing the *reaction mechanism* according to a suitable model. Several different functions are possible that represent according model concepts, e.g., reaction order, diffusion, 2D or 3D growth, etc. [32]. In the present paper, the focus is not on the determination of the actual mechanisms behind the reactions as this requires more detailed information on e.g. intermediate reaction steps or particle size. The goal of this study is rather to find suitable mathematical descriptions for the absorption and desorption reaction rate that can be used for

modelling of suitable reactors. Hence, the following three basic mechanisms are used corresponding to the observed decelerating, linear or sigmoidal behaviour in the transformed fraction versus time plots:

1st order (decelerating)
$$f(x) = (1 - x). \tag{5}$$

0th order (linear)
$$f(x) = 1. \tag{6}$$

general Avrami-Erofeev (sigmoidal)
$$f(x) = n(1 - x)[-\ln(1 - x)]^{\frac{n-1}{n}}. \tag{7}$$

For the determination of the different factors and parameters in Equation 3, isothermal reaction rate measurements are performed, and the following four fitting steps summarize the applied procedure [33]:

i. The thermodynamics of the reaction step is described by the van´t Hoff equation.

ii. The correct reaction mechanism for the reaction rate $f(x) = \frac{1}{k}\frac{\partial x}{\partial t}$ is determined. The mechanism is correct when the integral value versus the time follows a straight line, $g(x) = k \cdot t$. Then the slope refers to the rate coefficient *k*.

iii. In the next step, a correct pressure factor is determined: For each temperature and pressure, the associated rate coefficient *k* is divided by the values calculated for different pressure terms (see Equation 4). A sufficient fit is achieved when the values for experiments at the same temperature but different pressures match each other.

iv. In the last step, the activation energy E_a as well as the pre-exponential factor *A* are determined. According to $\ln\left(\frac{k}{f(P)}\right) = \ln A - \frac{E_a}{\mathcal{R}}\frac{1}{T}$, *A* refers to the exponent of the value of the intersection with the ordinate, while E_a refers to the slope times $\mathcal{R}$ when $\ln\left(\frac{k}{f(P)}\right)$ is plotted versus $\frac{1}{T}$.

This scheme is applied for the fitting procedure of all reaction rate equations presented in the following for absorption and desorption of the Li-Mg-N-H material. For all fitting procedures of the absorption and desorption data, the minimum and maximum range of fitted values for the transformed fraction has been set between 10 and 80 %, respectively.

3.3.1 Absorption reaction

The absorption experiments have been performed at three different pressures and up to five different temperatures

- 100 bar: (100), 125, 160 °C
- 85 bar: 125,150,160,170 °C
- 70 bar: (100), 125, 150 - repeat, 160, 170 °C

The first absorption experiments show good reproducibility. However, after the last experiment at 170 °C, the reaction rate decreased significantly, probably due to material degradation effects while the capacity remained constant. For the determination of model equations, the experiments after the degradation process have been excluded. The experiments at 100 °C have also been removed from the fitting procedure, as the measurements of the pressure signal have not been significant due to very slow reaction rates. For all remaining experiments, the experimental data have been fitted with

reaction rate equations for the first 1800 s. Furthermore, the data have been normalized referring to a maximum H_2 fraction of 3.2 wt.%. For longer timescales, the material is still absorbing some H_2. However, the reaction rate is very slow and in scale-up experiments, longer reaction times exceed the appropriate timeframe for an absorption experiment (e.g. automotive fuelling).

Figure 2 shows all experiments performed in one plot. Different colours indicate different pressures. It can be clearly seen that the reaction is rather slow below 150 °C. However, above this temperature, the rates increase very rapidly with increasing temperatures. At 170 °C, the absorption of the material can be completed in less than 5 minutes. It is very important to capture correctly this strong temperature dependency of the reaction rate, as the temperature behaviour in a lab-scale tank can be strongly non-isothermal due to heat transfer resistance of the powder material. Furthermore, Figure 2 indicates that besides the strong temperature dependency, the reaction rate also increases with increasing hydrogen pressure.

Referring to the literature [16], (compare Equation 2), the reaction proceeds in two steps and the according transition is indicated by the horizontal line in Figure 2.

The normalized transformed fraction of the first step of absorption ($X_{\mathrm{abs,I}}$) here refers to the first 33 % of transformed fraction x_{abs}, for the second step ($X_{\mathrm{abs,II}}$) to the following 67 %, respectively. The mathematical formulation of the normalization is $X_{\mathrm{abs,I}} = \frac{x_{\mathrm{abs}}}{0.33}$ for $0 \leq x_{\mathrm{abs}} \leq 0.33$ and $X_{\mathrm{abs,II}} = \frac{x_{\mathrm{abs}} - 0.33}{0.67}$ for $0.33 \leq x_{\mathrm{abs}} \leq 1$.

In order to follow the 4-step procedure described in Section 3.3, a description of reaction thermodynamics is required. In the present case, it is assumed that the thermodynamic data of both steps can be described by a single van´t Hoff equation, as experimental data are not available for a more detailed description. Even though this is a rather strong assumption, the resulting fits show a sufficient accuracy in the required temperature and pressure range. This is mainly due to the fact that all application relevant conditions are far from the thermodynamic equilibrium (P_{set} = 70 bar $P_{\mathrm{eq,abs}}$ < 20 bar for T < 170 °C). Thus, this empirical approach can be used in order to sufficiently describe the thermodynamic information in the reaction rate equations necessary for reactor design simulations. The according values refer to Section 3.2

$$\ln\left(\frac{P_{\mathrm{eq}}}{P_0}\right) = \frac{\Delta_R H}{\mathcal{R}T} - \frac{\Delta_R S}{\mathcal{R}}\ , \tag{8}$$

where P_0 is the reference pressure (1 bar). Using this information, the last three steps to fit the parameters for the empirical rate equations can be performed for both absorption steps.

3.3.1.1 1st absorption step

In the first step, just one reagent (i.e. gaseous hydrogen) that is very abundant is involved in the reaction, and the measured transformed fraction versus time data show a linear behaviour (see Figure 2). Therefore, a model with 0th reaction order has been chosen indicated by the factor of “1”. Furthermore, an Arrhenius-type temperature dependency as well as a dependency on the thermodynamic equilibrium have been included

$$\frac{X_{\mathrm{I,abs}}}{\partial t} = A_{\mathrm{abs,I}} \cdot \exp\left(-\frac{E_{\mathrm{a,abs,I}}}{\mathcal{R}T}\right) \cdot f(P, P_{\mathrm{eq,abs}}) \cdot 1. \tag{9}$$

Due to the 0th order characteristic of the reaction, the integral equation for the transformed fraction can be written as

$$g\left(X_{\mathrm{I,abs}}\right) = X_{\mathrm{I,abs}}(t) = k \cdot t, \tag{10}$$

where *k* refers to the rate coefficient

$$k = A_{\mathrm{abs,I}} exp\left(-\frac{E_{\mathrm{a,abs,I}}}{\mathcal{R}T}\right) \cdot \left(\frac{P - P_{\mathrm{eq,abs}}}{P_{\mathrm{eq,abs}}}\right). \tag{11}$$

By fitting a straight line to the transformed fraction versus time plot (Figure 2), this coefficient *k* can be determined as the corresponding slope. Additionally, using the second fitting step the pressure dependency of the reaction rate is determined. In this case, the best fit can be achieved, when the expression $f(P) = \left(\frac{P-P_{\mathrm{eq,abs}}}{P_{\mathrm{eq,abs}}}\right)$ is used. The corresponding Arrhenius plot, with the 95 % confidence intervals (dotted lines), is shown in Figure 3. Finally, by fitting a straight line to this data, the kinetic parameters can be determined: the slope refers to the effective activation energy $E_{\mathrm{a,abs,I}}$, and the intersection with the ordinate to the pre-exponential parameter $A_{\mathrm{abs,I}}$.

3.3.1.2 2nd absorption step

The determination of the rate equation for the 2nd reaction step is performed analogously. Figure 2, clearly shows that the evolution of the transformed fraction of this reaction step shows a decelerating behaviour. Therefore, a 1st order reaction has been assumed for the mathematical description of the reaction rate in this reaction step.

Complementing this term for the mechanism, again an Arrhenius-type temperature behaviour and a dependency on the thermodynamic equilibrium are included into the rate equation

$$\frac{\partial X_{\mathrm{abs,II}}}{\partial t} = A_{\mathrm{abs,II}} \cdot \exp\left(-\frac{E_{\mathrm{a,abs,II}}}{\mathcal{R}T}\right) \cdot f(P, P_{\mathrm{eq,abs}}) \cdot \left(1 - X_{\mathrm{abs,II}}\right). \tag{12}$$

According to the 1st order mechanism, the experimental data follow a straight line, when plotted according to the integrated rate equation

$$g\left(X_{\mathrm{abs,II}}\right) = -\ln\left(1 - X_{\mathrm{abs,II}}\right) = k \cdot t. \tag{13}$$

The slopes of these lines again refer to the rate coefficients *k*. The best fit for the pressure factor has been determined to $f(P) = \left(\frac{P-P_{\mathrm{eq,abs}}}{P_{\mathrm{eq,abs}}}\right)$, and the according Arrhenius plot with the 95 % confidence intervals (dotted lines) is shown in Figure 3.

The final full set of parameters for the rate equations of the two reaction steps is given in Table 1.

3.3.1.3 Discussion

The values for the activation energy presented in Table 1 are in the same range as literature values for the same reaction (128 kJ·mol^{-1} [21]). However, the errors in the activation energies, which refer to the exponent of the error in the slope of the straight lines, are rather large. Therefore, all values presented in Table 1 should not be referred to the actual physical properties, but to apparent values for a

sufficient fit of the effective reaction rate. Furthermore, these values are only valid in the measured temperature and pressure range and should therefore not be extrapolated.

Figure 4 A and B show the comparison between experimental and model data for the experiments at different temperatures and pressures of 70 and 85 bar, respectively. Changes in the slope of calculated curves for x_{abs} = 0.33 are related to the selected two step model. Obviously, the empirical two-step model is able to capture the temperature and pressure behaviour very well from 125 to 170 °C. Only in the first range of the 2nd reaction step for the experiments at temperatures above 150 °C, the model equations underestimate the experimental effects. This behaviour can be explained by very fast reactions leading to non perfect isothermal conditions in the reactor and thus faster reaction rates in the experiment. As a conclusion, it can be stated that the model can capture the temperature and pressure dependency of the absorption reaction rate. Therefore, it can be implemented into models that are used for tank design development. This has already been the case for studying the absorption reaction in a lab-scale reactor [5].

3.3.2 Desorption reaction

For desorption characterization, experiments have been performed at three different temperatures and up to four different starting pressures. The lowest starting pressures are indicated with “s.v.” for static vacuum at 5 mbar.

- 155 °C: s.v. (1.33 bar)
- 165 °C: s.v. (1.14), 1.4 (2.43), 3 (4.3) bar
- 175°C: s.v. (1.35), 1.4 (2.42), 3 (4.24), 4.5 (5.55) bar.

Results of experiments are shown in Figure 5 for the first 3600 s. For experiments with very slow rates, or experiments at high desorption pressures, at the end of an experiment the temperature has been set to 180 °C and the pressure to static vacuum (5 mbar) in order to guarantee full conversion. As the experiments have been performed in the Sieverts type apparatus described in Section 2, the pressures, which have been set in the beginning, increased by the additional hydrogen released during the experiment due to the compressed gas in the void fraction and due to the reaction, corresponding to approximately 1 bar and 0.9 bar, respectively. Therefore, the pressures set in parentheses indicate the pressure present in the system at 0.25 transformed fraction. These values are also used for the fit of the pressure dependency. Analogous to the absorption experiments, the maximum gravimetric capacity is 3.2 wt.%.

A summary of all measured transformed fraction as a function of time is given in Figure 5. From this plot, a clear sigmoidal shape of the curves can be observed, as well as a very slow reaction rate above 0.6 - 0.7 of transformed fraction. In accordance with the modelling of the absorption reaction, the desorption reaction is divided into two steps, where the transformed fraction of the first step $X_{des,I}$ refers to $0 \leq x_{des} \leq 0.67$ and for the second step $X_{des,II}$ refers to $0.67 \leq x_{des} \leq 1$, respectively.

Similar to the procedure for the determination of the rate equations of the absorption reaction, first a description of the thermodynamic equilibrium is necessary. These values differ from absorption due to a hysteresis behaviour of the reaction system and are summarized in Section 3.2.

3.3.2.1 1st desorption step

Due to the sigmoidal shape of the 1st reaction step, a model with a general Avrami-Erofeev mechanism is used for the mathematical description of the reaction rate in the present publication. For the variable *n* the best value has been determined to 1.5. Thus, the following equation describes the mechanism, the Arrhenius type temperature dependency as well as the pressure factor

$$\frac{\partial X_{\mathrm{des,I}}}{\partial t} = A_{\mathrm{des,I}} \cdot \exp\left(-\frac{E_{\mathrm{a,des,I}}}{\mathcal{R}T}\right) . f\left(P, P_{\mathrm{eq,des}}\right) \cdot \tag{14}$$

$$n\left(1 - X_{\mathrm{des,I}}\right) \cdot \left[-ln\left(1 - X_{\mathrm{des,I}}\right)\right]^{\frac{n-1}{n}}$$

The integrated form of this equation is

$$g\left(X_{\mathrm{des,I}}\right) = \left[-\ln\left(1 - X_{\mathrm{des,I}}\right)\right]^{\frac{1}{n}} = k \cdot t, \tag{15}$$

which is plotted in Figure 6 as a function of time. As the plotted data follows straight lines, the chosen mechanism sufficiently captures this reaction step, and the according slopes refer to the rate coefficients *k*. In this case, the thermodynamic contribution to the reaction rate is well described by a logarithmic pressure expression $f(P) = \ln\left(\frac{P_{\mathrm{eq,des}}}{P}\right)$. The corresponding Arrhenius plot is shown in Figure 7.

3.3.2.2 2nd desorption step

For the second desorption step, the fitting procedure is difficult as the rate of reactions are very slow leading to unsatisfying accuracies in the experiments. Therefore, the focus for the empirical rate equations has been to capture the behaviour in a very small temperature and pressure range that is most interesting for the coupling to a HT-PEM fuel cell, i.e. 165 °C and < 3 bar.

Analogous to the 1st absorption step, for the 2nd desorption step, a 0th order mechanism has been chosen resulting in a factor of “1” for the mechanism

$$\frac{\partial X_{\mathrm{des,II}}}{\partial t} = A_{\mathrm{des,II}} \cdot \exp\left(-\frac{E_{\mathrm{a,des,II}}}{\mathcal{R}T}\right) \cdot \mathrm{f}(P) \cdot 1. \tag{16}$$

As in the PCI diagrams a strong sloping region can be observed [10], the pressure factors for the 2nd desorption step represents a dependency of the maximum weight fraction on the final back pressure applied. With lower desorption pressures, higher storage capacities can be reached. The implemented function is therefore

$$f(P) = \left(1 - \frac{0.1515}{wt_{\max} \cdot 0.33}\ (P - 1.1[bar])\right) \cdot, \tag{17}$$

which is only valid for the technically relevant boundary condition of *P* < 7.7 bar. The according parameters for the Arrhenius type temperature dependency have been determined in analogy to the previous rate equations using only the experiments starting from static vacuum (5 mbar).

The final set of parameters for both steps is shown in Table 1.

3.3.2.3 Discussion

Figure 8 shows the experimental and simulated data for the 1st desorption step. From this plot it can be stated that the model is able to capture the measured data in the relevant range of transformed fraction quite well. Furthermore, Figure 9 shows experimental and simulated data for the complete desorption reaction at 165 °C with various back pressures. These parameters refer to the technically relevant conditions during a coupling procedure with a HT-PEM fuel cell. The agreement between the experimental data and the simulation using the empirical model equations is acceptable. However, it has to be emphasized, that the experimental data especially for the 2nd desorption step have been scarce. Therefore, any extrapolation to other temperatures should be avoided or checked carefully.

Finally, it can be concluded that the given desorption model equations are able to sufficiently describe the temperature, pressure and transformed fraction behaviour of the material in an application relevant range. Thus, the model equations can be used for solid state hydrogen storage tank design simulations.

4 Conclusions

Important parameters for the modelling of a hydrogen storage reactor based on $2LiNH_2$–$1.1MgH_2$-$0.1LiBH_4$-3wt.-%$ZrCoH_3$ have been determined. For the bulk density in the absorbed state a value of $1.00 \cdot 10^3$ kgm^{-3} has been measured for the as-milled sample and $0.79 \cdot 10^3$ kgm^{-3} for the desorbed state. Furthermore, the enthalpy and entropy of the absorption reaction have been determined to $\Delta_R H_{abs}$ = -38 kJ mol$^{-1}_{H2}$ and $\Delta_R S_{abs}$ = -111 J mol$^{-1}_{H2}$ K^{-1}, and for desorption to $\Delta_R H_{des}$ = 45 kJ mol$^{-1}_{H2}$ and $\Delta_R S_{des}$ 124 J mol$^{-1}_{H2}$K^{-1}, respectively.

Regarding the rate of reactions, for absorption, a 2-step model has been fitted to experimental data using a 0th order model for the first and a 1st order model for the second reaction step. The comparison between simulated and experimental data shows a good agreement, especially for the temperature dependence that is very important for the simulation of strongly non-isothermal solid state hydrogen storage tanks.

The desorption behaviour is best captured with an Avrami-Erofeev model using n = 1.5 for the first step, while for the second step a dependency of the transformed fraction on the equilibrium pressure has been included. Using these empirical equations, the first reaction step can be captured by the model equations over the experimentally determined temperature and pressure range. However, for the second step, the determined equations are just valid for the boundary conditions (~ 165 °C and < 3 bar) that occure during the coupling to a fuel cell.

In general, the given material data enables a complete mathematical description for the conversion of the reaction system $2LiNH_2$–$1.1MgH_2$-$0.1LiBH_4$-3wt.-%$ZrCoH_3$ at technically relevant boundary conditions that can be used for future tank simulation and development. An example for the application of these equations used in the model validation of a lab-scale tank is reported in [5,6].

5 Acknowledgements

The research leading to these results has received funding from the European Union's Seventh Framework Programme (FP7/2007-2013) for the Fuel Cells and Hydrogen Joint Technology Initiative under grant agreement n. 256653 (SSH2S).

6 Figures

Figure 1:

Left: photo of the reactor used for the reaction rate measurements consisting of container and spindle. Right: scheme of the Sieverts type testing setup.

Figure 2:

Transformed fraction vs. time for all absorption experiments. ■, □ (repro): 70 bar, ▲: 85 bar, ●: 100 bar. Temperatures as indicated by numbers and colours (black: 125 °C, blue: 150 °C, red: 160 °C, green: 170 °C). The horizontal line refers to the transition between 1^{st} and 2^{nd} reaction step.

Figure 3:

Arrhenius plots with experimental data (symbols) and fit with 95 % confidence intervals (straight and dashed line, respectively) for 1^{st} reaction step: ▲, and 2^{nd} reaction step: ■.

Figure 4:

Experimental (symbols) and model (lines) data for transformed fraction in both steps vs. time at indicated temperatures. A) at 85 bar B) at 70 bar.

Figure 5:

Transformed fraction vs. time plot for all experimental measurements at temperatures indicated by values and colours. s.v.: ■, 1.4 bar: ▲, 3 bar: ●, 4.5 bar: ▼.

Figure 6:

Experimental data and fit for reaction mechanism of 1^{st} desorption step. Initial pressures at s.v.: ■, 1.4 bar: ▲, 3 bar: ●, 4.5 bar: ▼. Temperatures at 175 °C: green: 165 °C red, 155 °C: black.

Figure 7:

Arrhenius plot for 1^{st} desorption step with experimental data (symbols) and fit (red line) as well as 95 % confidence intervals (dashed line).

Figure 8:

Transformed fraction vs. time for the 1^{st} reaction step of desorption. Symbols refer to experiments, lines to model equations. Black: 155 °C, red: 165 °C, green: 175 °C. s.v.: ■, 1.4 bar: ▲, 3 bar: ●, 4.5 bar: ▼.

Figure 9:

Transformed fraction vs. time for complete desorption experiments at 165 °C. Symbols refer to experiments, lines to model equations. s.v.: ■, 1.4 bar: ▲, 3 bar: ●.

7 Tables

Table 1:

Model parameters for 1st and 2nd reaction step of Li-Mg-N-H absorption (abs) and desorption (des) with according error values as well as the R^2 value for the quality of the fit.

Table 2:

Nomenclature

8 References

[1] Eberle U, Felderhoff M, Schüth F. Chemical and Physical Solutions for Hydrogen Storage. Angew Chem, Int Ed 2009;48(36):6608–30.

[2] Pfeifer P, Wall C, Jensen O, Hahn H, Fichtner M. Thermal coupling of a high temperature PEM fuel cell with a complex hydride tank. Int J Hydrogen Energy 2009;34(8):3457–66.

[3] Urbanczyk R, Peil S, Bathen D, Heßke C, Burfeind J, Hauschild K, et al. HT-PEM Fuel Cell System with Integrated Complex Metal Hydride Storage Tank. Fuel Cells 2011;11(6):911–20.

[4] Weiß-Ungethüm J, Bürger I, Schmidt N, Linder M, Kallo J. Experimental investigation of a liquid cooled high temperature proton exchange membrane (HT-PEM) fuel cell coupled to a sodium-alanate tank. Int J Hydrogen Energy 2013;submitted.

[5] Bürger I, Komogowski L, Linder M. Advanced reactor concept for complex hydrides: hydrogen absorption from room temperature. Int J Hydrogen Energy n.d.;submitted .

[6] Bürger I, Luetto C, Linder M. Advanced reactor concept for complex hydrides: hydrogen desorption at fuel cell relevant boundary conditions. Int J Hydrogen Energy n.d.;submitted .

[7] Zhang JJ, Xie Z, Tang Y, Song C, Navessin T, Shi Z, et al. High temperature PEM fuel cells. J Power Sources 2006;160(2):872–91.

[8] Corgnale C, Hardy BJ, Tamburello DA, Garrison SL, Anton DL. Acceptability envelope for metal hydride-based hydrogen storage systems. Int J Hydrogen Energy 2012;37(3):2812–24.

[9] Chen P, Xiong Z, Luo J, Lin J, Tan KL. Interaction of hydrogen with metal nitrides and imides. Nature 2002;420(6913):302–4.

[10] Luo W. ($LiNH_2$–MgH_2): a viable hydrogen storage system. J Alloys Compd 2004;381(1-2):284–87.

[11] Nakamori Y, Orimo S. Li–N based hydrogen storage materials. Mater Sci Eng B 2004;108(1-2):48–50.

[12] Aoki M, Noritake T, Nakamori Y, Towata S, Orimo S. Dehydriding and rehydriding properties of $Mg(NH_2)_2$–LiH systems. J Alloys Compd 2007;446-447:328–31.

[13] Luo W. Corrigendum to "($LiNH_2$–MgH_2): a viable hydrogen storage system." J Alloys Compd 2004;385(1-2):316.

[14] Moysés Araujo C, Scheicher RH, Ahuja R. Hydrogen Storage Materials. Appl Phys Lett 2008;92(2):021907.

[15] Luo W, Stavila V, Klebanoff LE. New insights into the mechanism of activation and hydrogen absorption of ($2LiNH_2$–MgH_2). Int J Hydrogen Energy 2012;37:6646–52.

[16] Weidner E, Dolci F, Hu J, Lohstroh W, Hansen T, Bull DJ, et al. Hydrogenation Reaction Pathway in $Li_2Mg(NH)_2$. J Phys Chem C 2009;113(35):15772–77.

[17] Hu JJ, Liu Y, Wu G, Xiong Z, Chua YS, Chen P. Improvement of Hydrogen Storage Properties of the Li–Mg–N–H System by Addition of $LiBH_4$. Chem Mater 2008;20(13):4398–4402.

[18] Yang J, Sudik A, Siegel DJ, Halliday D, Drews A, Carter RO, et al. Hydrogen storage properties of $2LiNH_2$+$LiBH_4$+MgH_2. J Alloys Compd 2007;446-447:345–49.

[19] Zhang X, Li Z, Lv F, Li H, Mi J, Wang S, et al. Improved hydrogen storage performance of the $LiNH_2$ MgH_2 $LiBH_4$ system by addition of ZrCo hydride. Int J Hydrogen Energy 2010;35(15):7809–14.

[20] Ulmer U, Hu J, Franzreb M, Fichtner M. Preparation, scale-up and testing of nanoscale, doped amide systems for hydrogen storage. Int J Hydrogen Energy 2012;38(3):1439–49.

[21] Hu JJ, Pohl A, Wang S, Fichtner M. Additive Effects of $LiBH_4$ and $ZrCoH_3$ on the Hydrogen Sorption of the Li-Mg-NH Hydrogen Storage System. J Phys Chem C 2012;116:20246–53.

[22] Janot R, Eymery J-B, Tarascon J-M. Investigation of the processes for reversible hydrogen storage in the Li–Mg–N–H system. J Power Sources 2007;164(2):496–502.

[23] Gross KJ, Carrington KR. Recommended Best Practices for the Characterization of Storage Properties of Hydrogen Storage Materials. Berkeley, California: 2008.

[24] Ruprecht D. Entwicklung, Konstruktion und Fertigung eines Reaktors zur Untersuchung der Kinetik von Metallhydriden. Hochschule Esslingen, Bachelor thesis, 2012, 2011.

[25] Blach TPP, Gray EMM. Sieverts apparatus and methodology for accurate determination of hydrogen uptake by light-atom hosts. J Alloys Compd 2007;446-447:692–97.

[26] Wang J, Keller J, Gross KJ. VI . A . 5 DOE Metal Hydride Center of Excellence. DOE Hydrogen Program 2005:487–527.

[27] Wang J, Liu T, Wu G, Li W, Liu Y, Araújo CM, et al. Potassium-modified $Mg(NH_2)_2$/2 LiH system for hydrogen storage. Angew Chem, Int Ed 2009;48(32):5828–32.

[28] Vyazovkin S, Burnham AK, Criado JM, Pérez-Maqueda LA, Popescu C, Sbirrazzuoli N. ICTAC Kinetics Committee recommendations for performing kinetic computations on thermal analysis data. Thermochim Acta 2011;520:1–19.

[29] Ron M. The normalized pressure dependence method for the evaluation of kinetic rates of metal hydride formation/decomposition. J Alloys Compd 1999;283(1-2):178–91.

[30] Luo W, Gross KJ. A kinetics model of hydrogen absorption and desorption in Ti-doped $NaAlH_4$. J Alloys Compd 2004;385(1-2):224–31.

[31] Mayer U, Groll M, Supper W. Heat and Mass transfer in metal hydride reaction beds: experimental and theoretical results. J Less Common Met 1987;131:235–44.

[32] Galwey AK, Brown ME. Thermal Decomposition of Ionic Solids. Amsterdam: Elsevier, 1st edition, 1999.

[33] Lozano G a., Ranong CN, Bellosta von Colbe JM, Bormann R, Fieg G, Hapke J, et al. Empirical kinetic model of sodium alanate reacting system (I). Hydrogen absorption. Int J Hydrogen Energy 2010;35(13):6763–72.

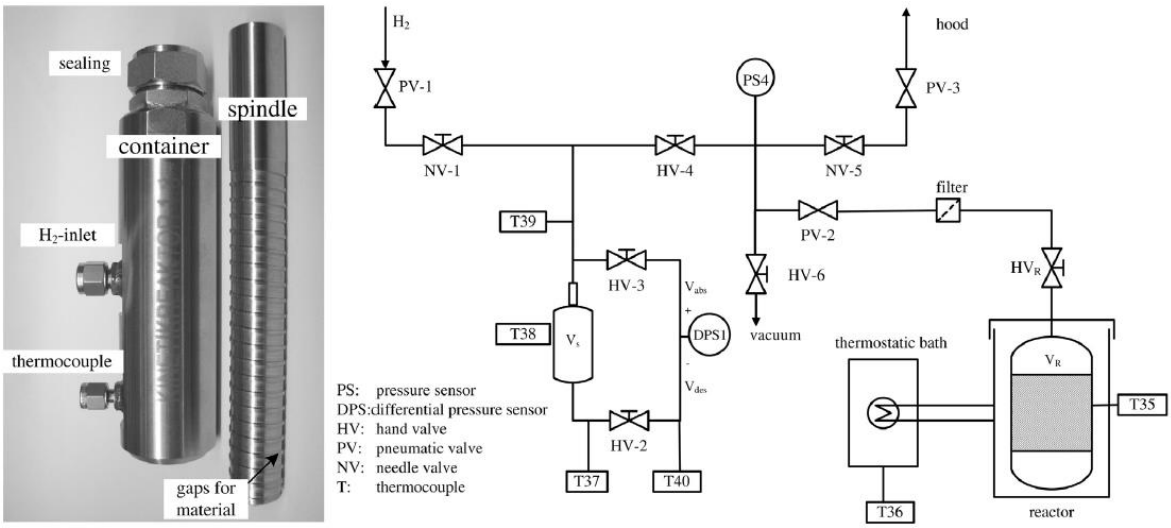

Table 1 – Model parameters for 1st and 2nd reaction step of Li–Mg–N–H absorption (abs) and desorption (des) with according error values as well as the R^2 value for the quality of the fit.

		Value	Accuracy
1st step abs $\left(\frac{P-P_{eq,abs}}{P_{eq,abs}}\right)$	$E_{a,abs,I}$ in kJ mol^{-1}	164.8	±4.6
	$A_{abs,I}$ in kJ mol^{-1}	$2.729 \cdot 10^{17}$	$\cdot e^{1.31} = 3.71$, $\cdot e^{-1.31} = 0.27$
2nd step abs $\left(\frac{P-P_{eq,abs}}{P_{eq,abs}}\right)$	$E_{a,abs,II}$ in kJ mol^{-1}	147.8	±7.9
	$A_{a,II}$ in kJ mol^{-1}	$4.678 \cdot 10^{14}$	$\cdot e^{0.95} = 2.59$, $\cdot e^{-0.95} = 0.39$
1st step des $\ln\left(\frac{P_{eq,des}}{P}\right)$	$E_{a,des,I}$ in kJ mol^{-1}	131.8	±7.1
	$A_{des,I}$ in kJ mol^{-1}	$2.35 \cdot 10^{12}$	$\cdot e^{1.92} = 6.82$, $\cdot e^{-1.92} = 0.15$
2nd step des	$E_{a,des,II}$ in kJ mol^{-1}	161.4	–
	$A_{des,II}$ in kJ mol^{-1}	$3.044 \cdot 10^{15}$	–

Table 2 – Nomenclature.

A	Pre-exponential factor	s^{-1}
E_a	Activation energy	kJ mol^{-1}
k	Rate coefficient	s^{-1}
P	Gas pressure	bar
P_0	Standard pressure	bar
P_{eq}	Gas pressure at equilibrium conditions	bar
$\Re$	Gas constant (8.314)	J kg^{-1} K^{-1}
s.v.	Static vacuum (here: 5 mbar)	
t	Time	s
T	Temperature	K
x	Transformed fraction	1
X_I	Transformed fraction of 1st step	1
X_{II}	Transformed fraction of 2nd step	1

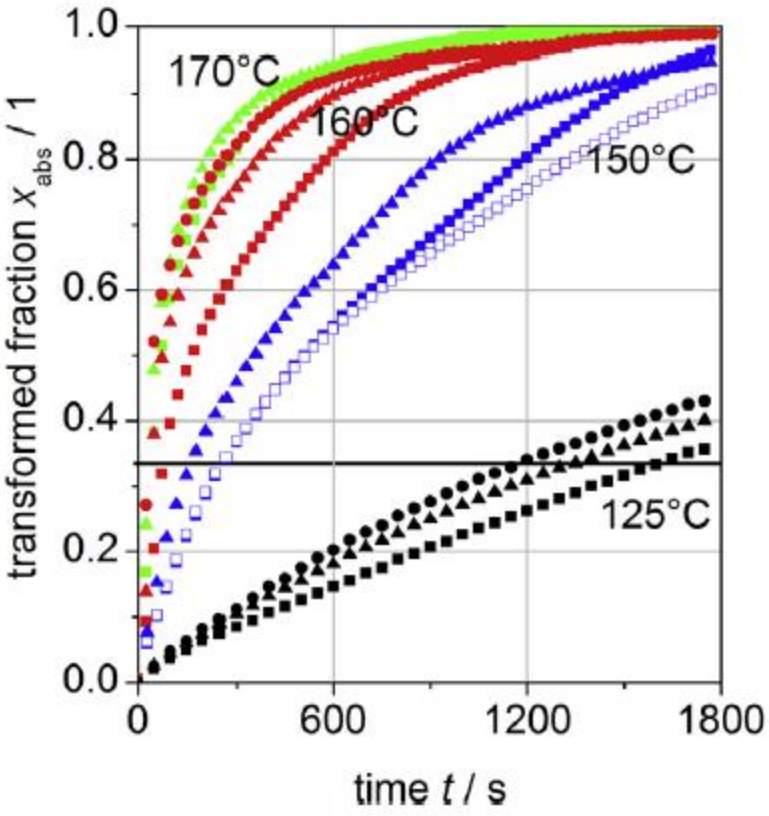

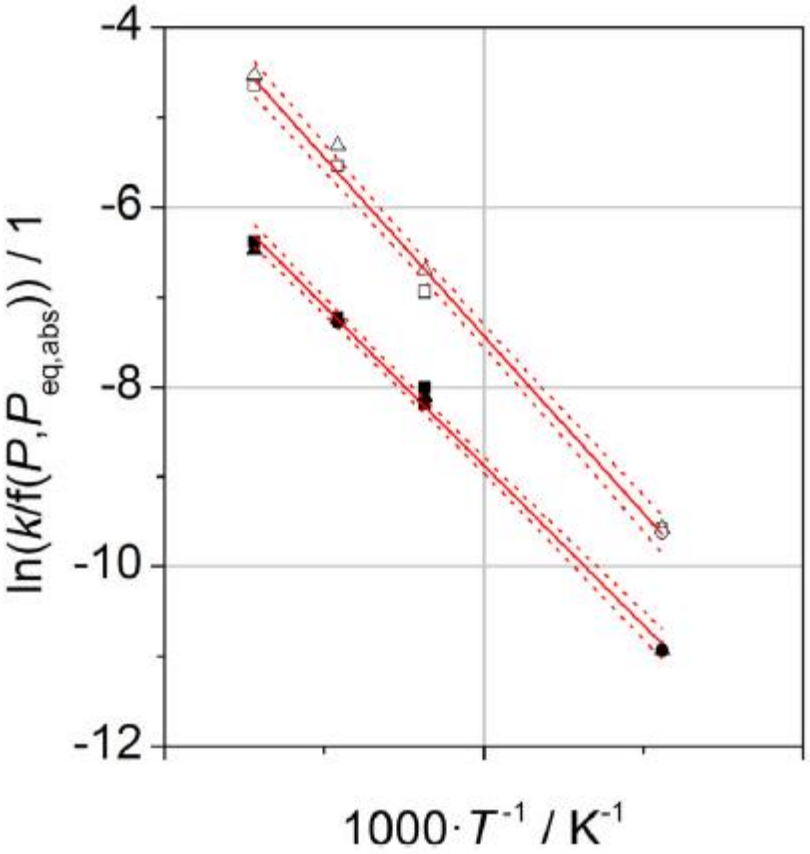
-4
-6
-8
-10
-12
ln(k/f(P,P_eq,abs)) / 1
1000·T^-1 / K^-1

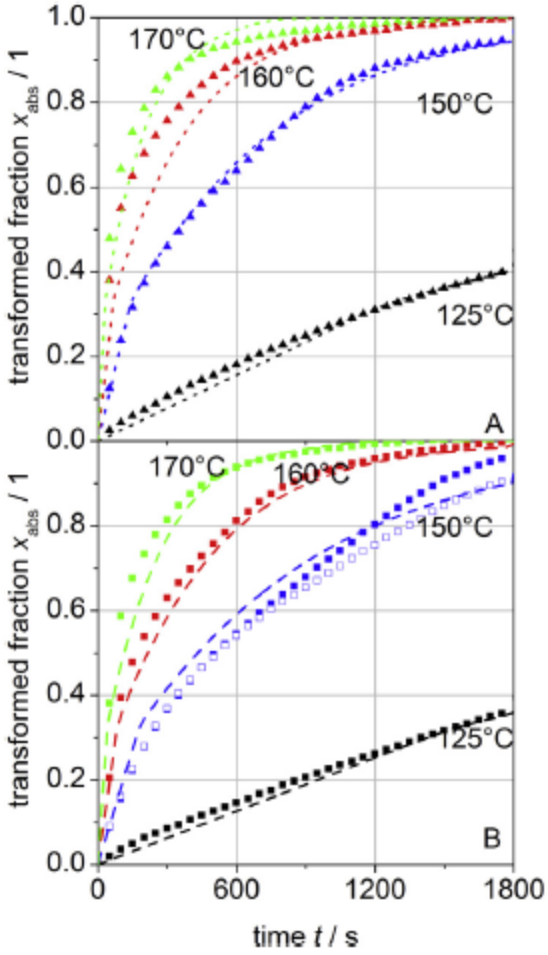
1.0
0.8
0.6
0.4
0.2
0.0
transformed fraction x_abs / 1
170°C
160°C
150°C
125°C
A
B
0
600
1200
1800
time t / s

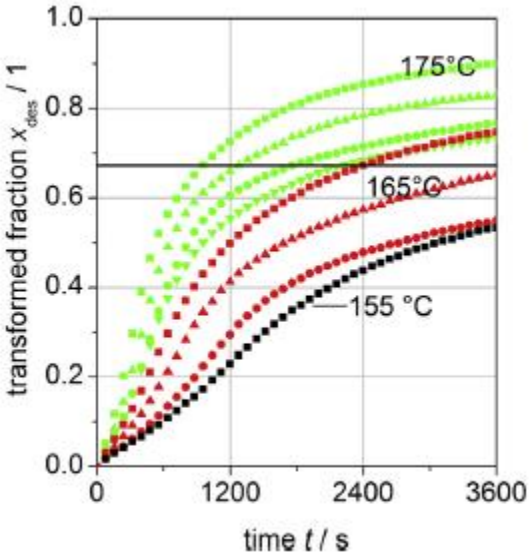
transformed fraction x_{des} / 1
time t / s
175°C
165°C
155 °C

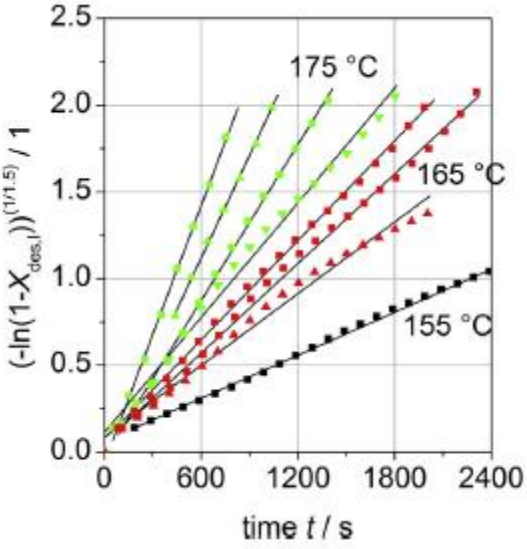
$(-\ln(1-X_{des,I}))^{(1/1.5)}$ / 1
time t / s
175 °C
165 °C
155 °C

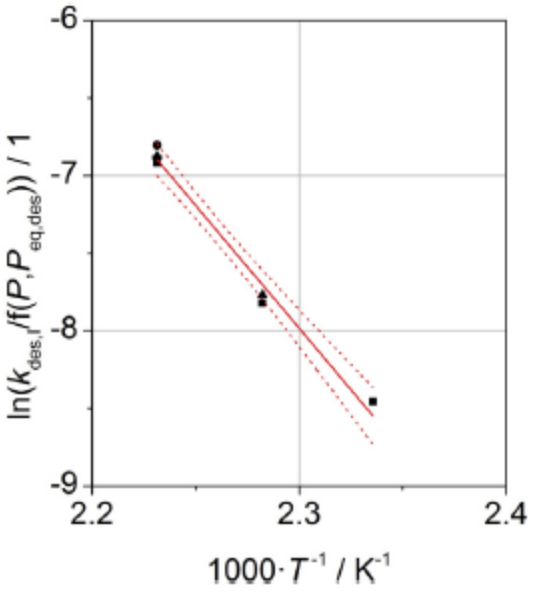
$\ln(k_{des,I}/f(P,P_{eq,des}))$ / 1
$1000 \cdot T^{-1}$ / K^{-1}

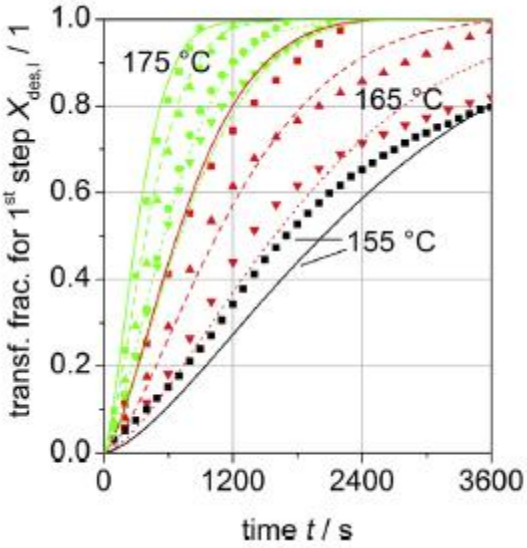
1.0
0.8
0.6
0.4
0.2
0.0
transf. frac. for 1st step $X_{des,I}$ / 1
175 °C
165 °C
155 °C
0
1200
2400
3600
time t / s

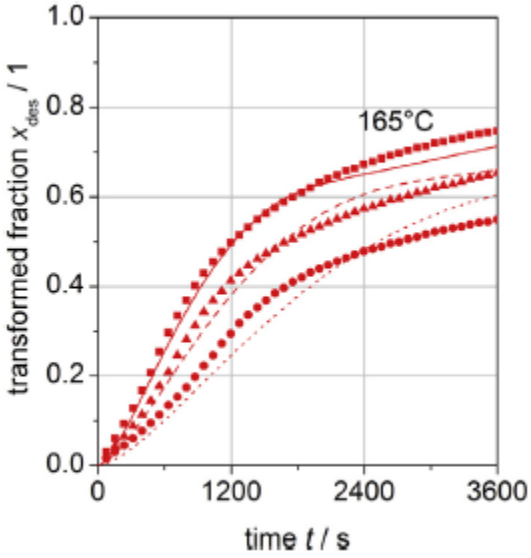
1.0
0.8
0.6
0.4
0.2
0.0
transformed fraction x_{des} / 1
165°C
0
1200
2400
3600
time t / s